JOURNAL OF AIRCRAFT
Vol. 33, No. 2, March–April 1996

Parachute Aerodynamics: An Assessment of Prediction Capability

James H. Strickland
Sandia National Laboratories, Albuquerque, New Mexico 87185
and
Hiroshi Higuchi
Syracuse University, Syracuse, New York 13244

Introduction

IN this Paper we review the present state of the art concerning the aerodynamic prediction capabilities for parachutes. Our review is confined to ballistic parachutes that primarily produce forces in the direction of motion as opposed to gliding parachutes, which may produce significant lift forces normal to the trajectory. We begin by discussing the general characteristics of parachute aerodynamics during deployment, inflation, and terminal descent. Basic bluff-body aerodynamics are next discussed in which relevant experimental observations and available numerical tools are noted. One of the most difficult aspects of parachute aerodynamics is modeling the inflation process. We examine several techniques that have been used for this purpose. We next consider several aerodynamic topics associated with deployment, steady descent, wake recontact, and aircraft/parachute interaction. We conclude by summarizing the present state of the art, noting current needs, and presenting possible future directions.

Characteristics of Parachute Aerodynamics

Deployment

The deployment process starts with the release of the parachute/payload system from the delivery system and ends with the initial inflation of the parachute. There obviously are many conceivable types of deployment that might occur from many different types of delivery systems. For example, at the RAeS/AIAA 12th Aerodynamic Decelerator Systems Technology Conference, parachute deployment schemes associated with reentry vehicles,[1] rocket boosters,[2] and cargo delivery from aircraft[3] were presented. Some of the better-known methods of initiating parachute deployment may be found in the 1963 Parachute Design Guide[4] and the 1978 Recovery Systems Design Guide.[5]

The deployment process is, in most cases, very complicated from an aerodynamic standpoint. The flow is unsteady and there is usually a coupling between aerodynamic forces and the system dynamics. In addition, the state of the flowfield into which the deploying parachute system is being inserted may be important. For example, in the cargo extraction schemes studied by Behr,[3] the wake of the C-17 aircraft must be considered when assessing the performance of parachutes that are being used for the extraction of a series of cargo containers.

Inflation

Inflation of the parachute begins with the introduction of fluid into the mouth of the canopy. As the canopy changes shape, new pressure distributions are produced on the inside and outside of the canopy. This, in turn, causes the canopy shape to continue to change. The canopy geometry, material, and construction are all integrally related to the inflation process. Because of stretching of the material, not only can the gross geometry change, but the porosity of the material may also change.

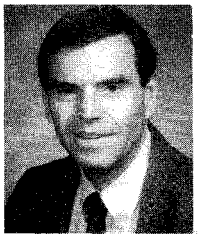

Dr. J. H. Strickland is a Distinguished Member of the Technical Staff in the Engineering Sciences Center at Sandia National Laboratories. Dr. Strickland received his B.S. in Mechanical Engineering from Texas Tech University and his M.S. and Ph.D. in Mechanical Engineering from Southern Methodist University. He began his career designing small gas turbine and jet engines for Boeing and GE. Prior to coming to Sandia National Laboratories, he was a Professor of Mechanical Engineering and Associate Dean of Engineering at Texas Tech University. He has pioneered analysis tools for the prediction of the three-dimensional flowfields around vertical axis wind turbines and high-performance parachute systems using vortex and integral momentum analysis techniques. He is an Associate Fellow of AIAA and a Member of ASME and ASEE.

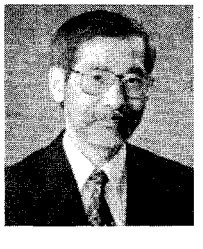

Dr. Hiroshi Higuchi received his B.S. degree from the University of Tokyo in 1970 and his M.S. and Ph.D. degrees in Aeronautics from California Institute of Technology in 1971 and 1977, respectively. He worked at NASA Ames Research Center as a principal investigator from 1976 until 1981 after which he taught and conducted research at the University of Minnesota. He is presently a Professor of Aerospace Engineering at Syracuse University. He received a NASA Space Act Award for his contributions in wall shear stress measurements and his flow visualization studies have received citations from the American Physical Society. He is an Associate Fellow of AIAA and a Member of ASME, APS, and ASEE.

Presented as Paper 95-1531 at the AIAA 13th Aerodynamic Decelerator Systems Technology Conference, Clearwater Beach, FL, May 15–18, 1995; received June 9, 1995; revision received Oct. 31, 1995; accepted for publication Nov. 20, 1995.

The canopy forces are determined not only by the aerodynamic pressure distributions, but also by the forces transmitted to the canopy by the suspension lines. The forces in the suspension lines are, in turn, a function of the dynamics and gravitational loads associated with the payload. In many cases, the parachute system is deployed horizontally and inflation begins while in that position. Eventually, the system turns over such that the alignment of the parachute system is vertical. The payload will usually, but not always, be decelerating during the inflation process. The inertia of the canopy itself also may influence the inflation process.

In summary, inflation is a complex process in which the fluid dynamics are coupled to the system dynamics. The grand challenge with regard to simulating the inflation process is to be able to predict the pressure distribution on the canopy as a function of time and position on the canopy.

Terminal Descent

Parachute systems that are deployed at sufficient altitudes above the ground will eventually reach some terminal descent velocity. Even under the best circumstances, however, the flowfield is unsteady in the wake region. This appears to be a characteristic of most, if not all, bluff bodies at modest to high Reynolds numbers. This unsteadiness is born out by numerous flow visualization studies of bluff bodies. We will review some of these observations in a subsequent section. Those who run steady-state computational fluid dynamics (CFD) codes on bluff bodies often are puzzled by the lack of convergence to a steady state.

There are other unsteady phenomenon that have been observed during terminal descent. For canopies that have low geometric and material porosities, one may observe a coning oscillation in which the vent of the parachute rotates around a circle whose center is on the vertical axis. The range of angles associated with this oscillation is quantified for various types of parachutes in the Recovery Systems Design Guide.[5] Puffing motions have been observed for low-porosity flat circular parachutes. In this case, the skirt diameter oscillates in a periodic fashion about some mean value. The drag coefficient also oscillates about some mean value because of the change in drag area. Note also that spatial and temporal variations in the wind play a role in the unsteadiness during terminal descent. The ultimate effect on the system dynamics is, of course, a coupled one in which the unsteady aerodynamic forces affect the motion of the fore body which, in turn, affects the motion of the parachute and the aerodynamic forces on it.

Bluff-Body Aerodynamics

General Characteristics

Flows over bluff bodies are accompanied by large-scale flow separations and contribute to high drag forces. Parachute designers choose bluff-body geometries for their high drag force, but at the same time must cope with massively separated unsteady flow characteristics associated with such geometries. The wake of a bluff body at a moderate-to-high Reynolds number is dominated by unsteady turbulent vortex motions. In spite of the prevalence of this phenomenon and the extensive research it has inspired (note the bluff-body wake is found even in da Vinci's sketch book), many questions about it remain unanswered, even in the case of simple geometries.

The most fundamental geometries of bluff bodies are the two-dimensional flat plate and the circular or rectangular cylinder placed normal to the flow. In both cases, asymmetric vortex shedding occurs for any modest-to-high Reynolds number. The Reynolds number dependency of the flow pattern and von Kármán vortex streets in their wakes are well known. However, recent studies have demonstrated the inherently three-dimensional nature of both the vortex shedding and the wake structures behind the nominally two-dimensional or moderately three-dimensional circular cylinder. See, for example, the article by Bearman.[6]

Some insight into parachute aerodynamics may be obtained by examining flow over simple axisymmetric shapes such as disks, cups, and even spheres. The wake of a bluff body is inherently unstable because of the presence of a recirculation bubble and the accompanying reverse flow. The nature of the instability has been studied numerically and analytically, and the most unstable mode is found to be nonaxisymmetric. A recent article by Natarajan and Acrivos[7] gives a detailed study for the axisymmetric disk flow. The results of stability analysis confirm the fact that the flow will be dominated by nonaxisymmetric wake motions. As will be shown later, the wake behind an unvented bluff body remains axisymmetric only during the early stage of starting flow.

Experimental Observations

Our review of experimental studies on bluff bodies is limited primarily to the wake behind axisymmetric geometries pertinent to parachute aerodynamics. Planar two-dimensional configurations are generally excluded. Basic experiments have focused on rigid bodies. While numerous test results exist on model parachutes and full-scale parachutes, the flowfield survey behind flexible canopies is difficult and awaits future study. Drag force and surface pressure measurements on cloth parachute models and hemispherical cups are summarized by Maydew and Peterson.[8]

The structure of the steady-state wake behind axisymmetric bodies has been studied extensively. In addition, the steady-state drag and surface pressure distributions have been measured on these geometries. Roos and Willmarth[9] presented a drag coefficient for a disk over a wide range of Reynolds numbers. The drag coefficients of various bluff bodies are summarized by Blevins.[10]

Paradoxically, one of the simplest rigid bluff bodies placed in a steady incoming flow produces an extremely complex wake flow. The time-dependent wake structure behind a sphere has been experimentally investigated.[11-13] Recent experiments on the wake structure behind a disk include those by Fuchs et al.[14] and Berger et al.[15] Typically, three types of unsteady motion are found in the wake. The lowest frequency motion takes the form of axisymmetric breezing, or puffing, in the recirculation region. The predominant structure is caused by the three-dimensional helical or plane symmetric vortex shedding. The frequency of vortex shedding typically corresponds to the Strouhal number, in the range of 0.13–0.16. The shear-layer instability, much higher in frequency and highly Reynolds number dependent, can be detected in the region of the separating shear layer behind the shoulder of the model. Berger et al.[15] also studied the effects on the wake structure from various motions imposed on the disk. For example, Fig. 1 shows a wake behind a disk undergoing a small nutation excitation.

Any porosity of the bluff body suppresses the large-scale vortex motion behind axisymmetric geometries, as has been experimentally observed by Higuchi[16] and Cannon.[17] Porosity effects have long been exploited by parachute designers in their use of ribbon and ring-slot canopies. The near-wake structure behind these apertures can be relatively convoluted as the resultant jets merge in an irregular pattern. This flow interaction is a likely cause for a seemingly paradoxical increase in drag when a disk is provided with a small opening or low porosity as observed by Roberts[18] and Hoerner.[19] Even though the mean velocity profiles in the far wake of solid or porous bluff bodies possess a similar Gaussian profile, the near-wake pattern is strongly dependent on the bluff-body geometry.

The parachute canopy is generally equipped with a vent at its apex, which helps to control the inflation process and to stabilize the near-wake region. The effect of a base bleed on a sphere was studied recently by Suryanarayana et al.[20] Even with an extremely small opening through the centerline, they observed a reduction of drag as well as suppression of asymmetric wake oscillations. Bearman and Takamoto[21] conducted

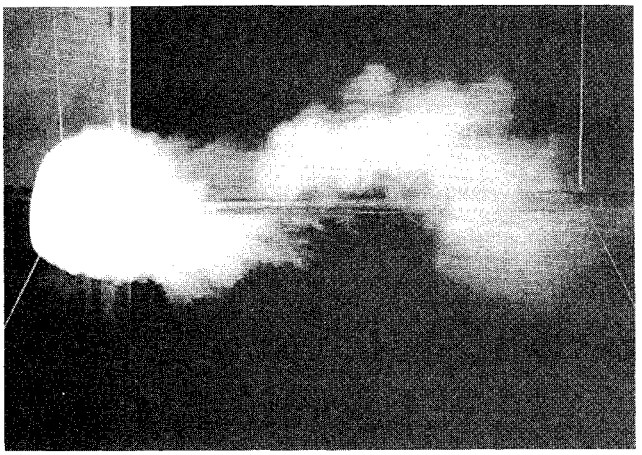

Fig. 1 Near wake behind a nutating disk.[15]

Fig. 2 Smoke visualization of parachute flight test.[8]

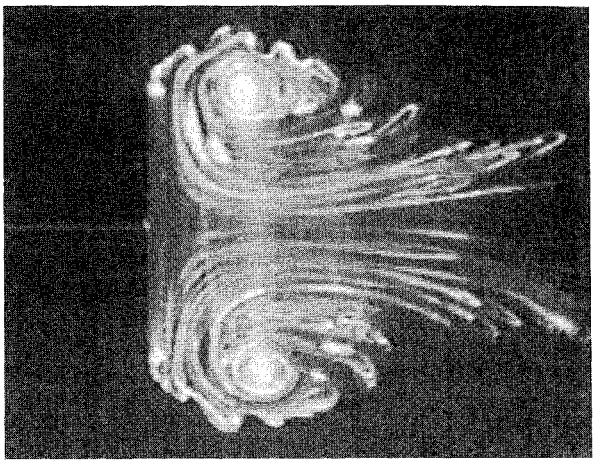

a)

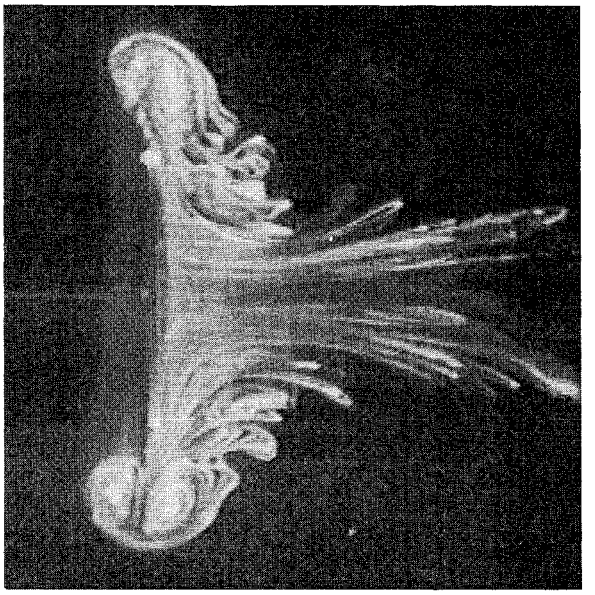

b)

Fig. 3 Wake behind a decelerating disk.[24,25] T = a) 3.4 and b) 4.0.

a wind-tunnel experiment behind bluff rings of different widths. They estimated the vorticity field and compared it with that behind a disk. When the i.d. of the ring was increased to about 70% of the o.d., the wake structure was comprised mainly of periodic axisymmetric vortex rings.

The studies quoted previously were conducted in small-scale laboratory settings. An example showing wake structure behind a full-scale parachute, which is taken from Maydew and Peterson,[8] is shown in Fig. 2. In this figure, a 13-ft-diam lifting parachute was released from an F-4 aircraft at approximately 320 m/s. The narrow wake from the store prior to the parachute deployment contrasts with the large-scale three-dimensional wake structure at $t = 1.99$ s. Though the wake structure is somewhat altered by the asymmetric porosity of the canopy, the smoke exhibits the three-dimensional helical structure, which is quite similar in overall shape and wavelength to those observed behind simpler axisymmetric bluff-body models such as the disk, which is shown in Fig. 1.

Except during its final descent stage, a parachute is subject to a relative freestream velocity, which is highly time dependent. At the initial opening of a canopy, large ring vortices are produced and a large drag force is encountered. After the initial inflation, a parachute canopy undergoing rapid deceleration may collapse partially or completely as the initial wake overtakes the canopy. This phenomenon is called the wake recontact and will be discussed in more detail in a later section. Flow experiments that illustrate this phenomenon for two-dimensional geometries were conducted by Sarpkaya et al.[22] and Oler et al.[23] to gain physical insights into this problem. Higuchi[24] and Balligand and Higuchi[25] studied the flow behind a disk rapidly accelerated to a constant speed, then decelerated to a secondary speed. Figure 3a shows a cross-sectional view of the wake after startup. Here, T is the nondimensional time normalized by the disk diameter and the constant velocity. The formation of an axisymmetric vortex ring is clearly seen in this figure. Shortly after the disk starts to decelerate, the vortex moves closer to the disk and increases in diameter. In Fig. 3b, the wake overtakes the disk, producing a counter-rotating vortex ring. As will be shown later, this flowfield is accompanied by a large negative drag. Note that the wake structure remains axisymmetric. When the disk is subjected to a steady incoming flow for a longer period of time, the vortex structure undergoes three-dimensional deformations and eventually three-dimensional shedding begins.

The studies mentioned previously were primarily conducted in subsonic regimes. In experiments with parachute models at low Mach numbers, the flowfield has been shown to be only mildly sensitive to forebody geometry, as long as the forebody is of a modest scale relative to the parachute. For this reason, the effect of the forebody on the parachute aerodynamics is usually ignored. On the other hand, for supersonic Mach numbers, the geometry and placement of the forebody relative to the parachute will have a dramatic effect on the flow, which impinges on the parachute itself. Therefore, supersonic para-

chute aerodynamics should be discussed only as a fully configured system. For additional information on supersonic flow over a parachute, the reader is referred to Maydew and Peterson.[8]

Numerical Prediction of Bluff-Body Flows

There are two classes of numerical tools that allow one to calculate the flow over bluff bodies, conventional grid-based CFD models and vortex element methods (VEM). There are advantages and disadvantages associated with both methods. These two approaches will be discussed in a very general way and no attempt will be made to provide a comprehensive review of either method. Several example calculations will be presented. In-depth treatments of modern grid-based CFD methods are given in Refs. 26–28. Vortex element methods and underlying principles are discussed in-depth in recent works.[29–31]

The relative merits of conventional CFD methods over VEM include the fact that there are a number of commercially available codes such as FIDAP™, NEKTON™, NACHOS™, and CFD-ACE™ for incompressible flows; and FLUENT™, RAMPANT™, and FLOW-3D™ for compressible flows. To properly resolve the flow, one must include a significant portion of the wake region in the calculation. To properly resolve the wake structure and reduce the effects of numerical diffusion, the wake region must be finely gridded. In addition, since the body is bluff, the upstream and lateral mesh boundaries must be a significant distance from the body, especially for low Mach number flows. If the bluff body is flexible or articulates, the flow may have to be regridded at every time step. Thus, the computational costs will be high using grid-based techniques.

The advantage of VEM is that vortex elements need be placed only in regions where vorticity is present. The flowfield for a divergence-free flowfield is completely described by the vorticity field. In addition, there is no numerical diffusion associated with the transport of vorticity. The greatest disadvantage of VEM is that commercial codes are, in general, not available for bluff-body flows. There are, on the other hand, several vortex panel codes such as VSAERO™ and USAERO™ that are used in calculating aircraft, auto, and marine flows. These codes generally give excellent results when there is no flow separation. Flow separation is handled in several ways, which include making integral boundary-layer calculations and simple user specification of separation points/lines. The accuracy of these calculations when separation occurs is in many cases questionable.

An interesting comparison between a conventional CFD code and a vortex code for flow over a rotating cylinder has been made by Clarke and Tutty.[32] Streamlines computed by Clarke and Tutty[32] using VEM are shown in Fig. 4, whereas the grid-based CFD computation by Badr et al.[33] is shown in Fig. 5. The cylinder has been impulsively started from rest and has moved 5.5 diameters in the flow. The tangential surface velocity of the cylinder is one-half of the translational speed. The Reynolds number based on the diameter is 1×10^3. The agreement between Figs. 4 and 5 is seen to be excellent.

Streak-lines for a companion flow visualization experiment for the impulsively started rotating cylinder Badr et al.[33] are shown in Fig. 6. While no direct comparison between streamlines and streak-lines can be made, it is clear that the general nature of the calculated flow is born out by the flow visualization experiment.

A vortex method that is capable of solving the axisymmetric flowfield over bluff bodies consisting of thin shells such as disks, partial spheres, rings, and other such shapes is given by Strickland[34] and is implemented in the computer code VPARA. Ring vortices are shed along the surface at each time step such that the normal and tangential velocity boundary conditions are satisfied. This technique requires relatively large numbers of ring vortices (1000–8000) to obtain good simulations. Since the direct calculation of perturbations from large numbers of

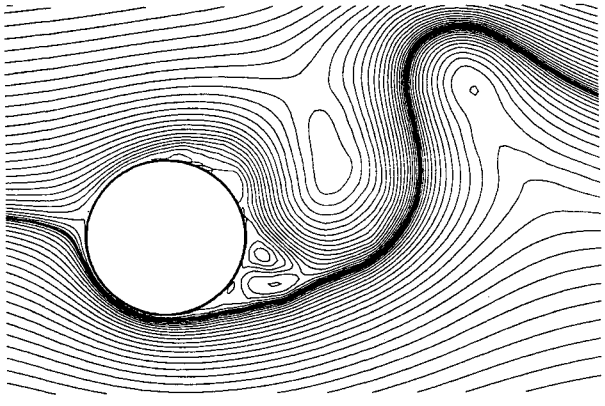

Fig. 4 Translating/rotating cylinder, vortex calculation.[32]

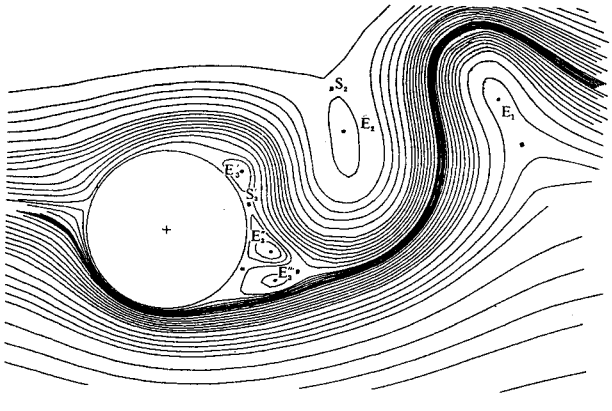

Fig. 5 Translating/rotating cylinder, conventional CFD calculation.[33]

Fig. 6 Translating/rotating cylinder, experimental.[33]

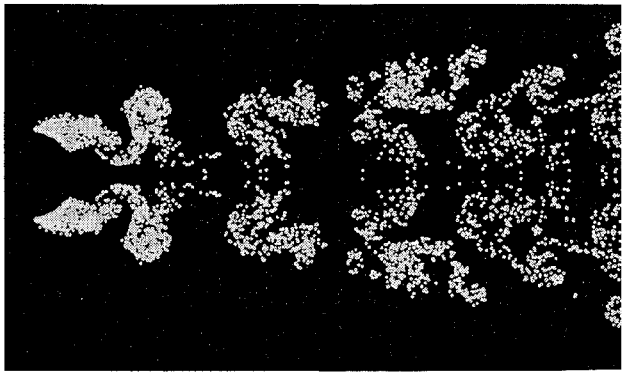

Fig. 7 Wake behind a hemispherical shell with a 40% vent.[34]

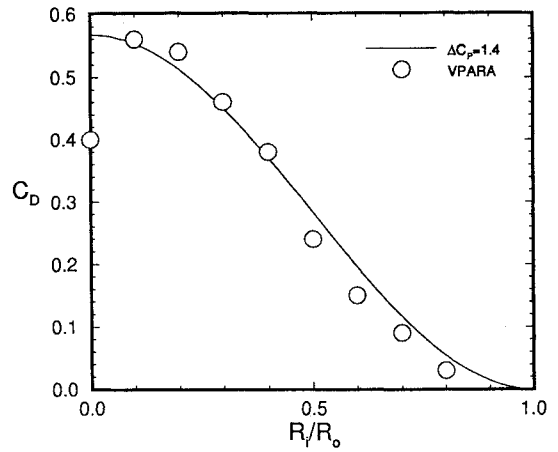

Fig. 8 Vented hemispherical shell drag coefficients.[34]

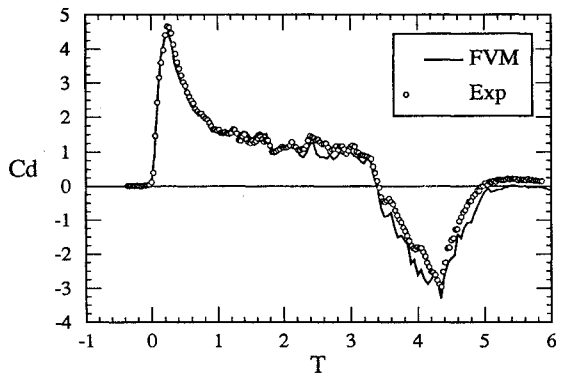

Fig. 9 Unsteady disk drag.[35]

ring vortices is computationally intensive, a fast multipole method was used to greatly reduce computer processing time.

A typical VPARA calculation for the wake flow over a hemisphere with a vent is shown in Fig. 7. The vent radial length is 40% of the hemisphere radial length (R_i/R_0 = 0.40). The term radial is the standard term used in parachute construction. As can be seen from this figure, a number of periodic structures have been shed from the vented hemispherical shell. This results in pronounced periodicity in the drag coefficient time history. The nondimensional fluctuation period $U_\infty \tau/R_0$ is equal to about 2.0.

The drag coefficient C_D is shown in Fig. 8 as a function of R_i/R_0. This drag coefficient is based upon the area πR_0^2 and the velocity U_∞. To estimate the steady-state drag obtained from the numerical simulations, the drag data were averaged over the last 120 time steps. The drag coefficient for a hemispherical shell based on the projected frontal area is approximately 1.4. Therefore, the drag coefficient based on the area πR_0^2 is equal to 0.567. For a hemispherical shell with a small vent, one might assume that the pressure distribution along the surface is essentially that of the shell without a vent, except very near the vent itself. If one further assumes that the pressure coefficient ΔC_P is a constant value of 1.4 along the surface, an estimate of the drag coefficient for a vented hemispherical shell can be made. From Fig. 8 it can be seen that the VPARA results are correlated remarkably well with this estimate, except for shells with very large vent ratios.

The presence of the anomalous VPARA prediction at R_i/R_0 = 0, as compared to reasonable results at other vent ratios for the hemispherical shell, can be explained by observing that while the wake is initially axisymmetric, it eventually becomes asymmetric, which tends to remove the buildup of vorticity from the downstream surfaces, resulting in a higher drag coefficient. The presence of the vent tends to not only preclude the buildup of vorticity from the downstream surfaces, but it may also stabilize the flow and either prevent asymmetry or at least move the asymmetry far enough downstream such that it does not affect the local flowfield near the body.

Higuchi et al.[35] present a set of calculations and companion data for flow over a disk that is first accelerated from rest to a constant velocity and then decelerated to a second constant velocity. The computations were made using the VPARA code. The drag coefficient for a case in which the disk is decelerated to rest is shown in Fig. 9. The solid curve labeled FVM is the VPARA calculation. The agreement is seen to be excellent.

A VPARA calculation[34] for the time-averaged drag of a disk in steady flow has been shown to be too low just as in the case of the hemispherical shell. On the other hand, the time-averaged drag calculations[34] for vented disks in a steady flow agree well with experimental data. One is led to believe that the axisymmetric assumption is valid for cases where the time period of simulation is not too long and for cases where the axisymmetric shell is vented.

An example of a flow calculation with a complicated parachute geometry is presented by Nelsen.[36] Steady-state calcu-

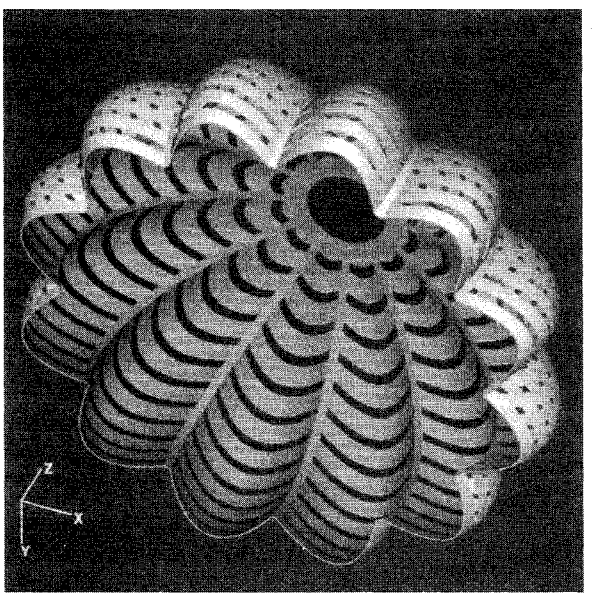

Fig. 10 CFD calculation for flow over a 12-gore, 12-ribbon parachute.[36]

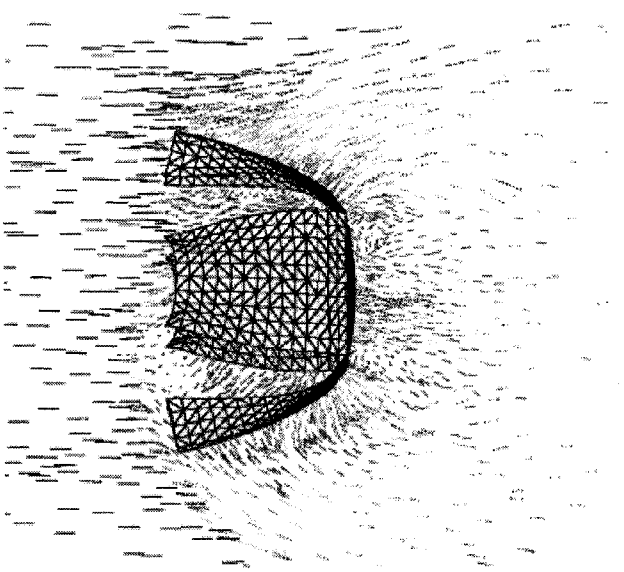

Fig. 11 CFD calculation for flow over a cross parachute.[26]

lations for the rigid 12-gore parachute canopy shown in Fig. 10 in both subsonic and supersonic flow were made using the CFD code RAMPANT.

A recent calculation made by Nelsen for a cross parachute is shown in Fig. 11. In this example, the general shape of the parachute was first calculated using the structural code ABAQUS™. The flow was then calculated using RAMPANT and the shape adjusted to match the new pressure distribution. A second and final flow calculation was then made.

Another iterative calculation has been made for the steady flow over a half-scale, 28-gore, C-9 solid cloth parachute by Sahu et al.[37] In this study the CFD code INS3D developed by Rogers et al.[38] was used in conjunction with Sundberg's[39] CALA canopy structural code.

Inflation Models

Simple Axial Momentum Models

Our discussion on empirically based axial momentum inflation models is very brief, but hopefully will capture the spirit of these methods. The interested reader is referred to Knacke,[40] who presents a detailed discussion of empirically based modeling methods for the inflation process.

The aerodynamic force along the axis of symmetry of the parachute is typically expressed by

$$F_x = \frac{1}{2}\rho(C_D S)U^2 + \frac{\mathrm{d}}{\mathrm{d}t}(m_a U) \tag{1}$$

where ρ is the fluid density, C_D is the drag coefficient, S is a drag area, U is the velocity of the parachute along its axis of symmetry, and m_a is the added mass associated with the fluid. This force is balanced by the inertial and gravitational loads of the system along the parachute symmetry axis.

In the simplest case, it is assumed that the parachute stays aligned with the trajectory and that C_D is a constant. The added mass m_a is assumed to be a function of the parachute geometry, perhaps proportional to the cube of the parachute diameter. The variation of the area S with respect to time must also be specified. For instance, one might assume that the area S changes in a linear fashion from some initial value to some final value in some time t_f. Here, t_f is an empirically based fill time. Thus, the use of the two empirical constants C_D and t_f along with simple formulations for the added mass and drag area would allow one to solve the equation of motion along the trajectory.

There is a considerable database for determining appropriate values for C_D and t_f, as well as for calculating m_a and modeling the change in S. This database considers a large number of geometric properties of the parachute, including basic constructued shapes, reefing, and porosity, as well as variables associated altitude, dynamic conditions at line snatch, and terminal velocity. The nature of some of these correlations may force one to solve the equations of motion in an iterative fashion.

Simple, empirically based axial momentum methods for obtaining gross design loads and timing sequences during inflation are broadly utilized because of their ease of use. It is expected that these methods will continue to play a major role for preliminary design studies.

Axial and Radial Momentum Models

In the previous axial momentum model, t_f had to be specified along with assumptions concerning the variation of S during the fill time. Wolf[41] and McVey and Wolf[42] developed an early model that included a radial momentum equation designed to eliminate the need to specify these parameters. More recently, Macha[43] has improved the method, making it more reliable.

The basic canopy model conceived by Macha[43] is shown in Fig. 12. In this model, the outward radial force F_r produced

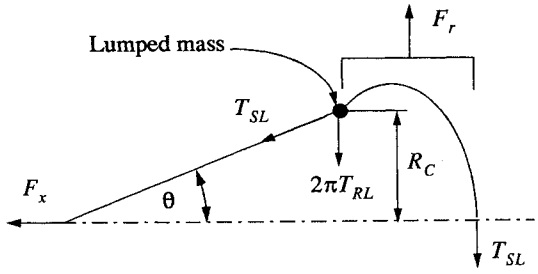

Fig. 12 Canopy force model.[43]

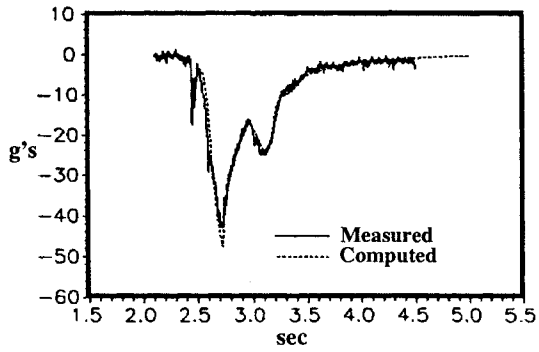

Fig. 13 Calculated and measured acceleration histories for 26-ft-diam parachute.[43]

by the fluid is assumed to act at the skirt of the parachute and is given by

$$F_r = \frac{1}{2}\rho(C_r S)U^2 - \frac{1}{2}\rho C_r S|\dot{R}_C|\dot{R}_C - \frac{\mathrm{d}}{\mathrm{d}t}(m_r \dot{R}_C) \tag{2}$$

where C_r is analogous to a radial drag coefficient, $\dot{R}_C$ is the time rate of change of R_C, and m_r is a radial added mass.

The first term on the right-hand side (RHS) is equivalent to the integrated radial force because of the stagnation pressure acting on the canopy, whereas the second term on the RHS reflects a loss in that pressure because of the radial motion of the canopy. The last term in Eq. (2) represents the radial force required to accelerate the fluid radially.

From Fig. 12 note that the suspension line tension T_{SL} has both axial and radial components, which enter into the axial and radial momentum equations, respectively. The momentum equations are also coupled by the freestream velocity U.

The novelty of Macha's approach, however, has its basis in the fact that the reefing line tension T_{RL} can be used to obtain values for $C_r S$ from steady wind-tunnel tests as a function of $C_D S$:

$$C_r S = (C_D S)\frac{1 + \sin\theta}{\cos\theta} + 4\pi\frac{T_{RL}}{\rho U^2} \tag{3}$$

He further assumed that the radial added mass is of the form

$$m_r = \rho k_r V \tag{4}$$

where k_r is an added mass coefficient, and V is the volume of fluid contained within the parachute canopy. Macha obtained a correlation for the radial-added mass coefficient as a function of the ratio of the instantaneous diameter to the full open diameter and the ratio of the initial velocity to the terminal velocity.

Macha's computer code MIMIC has been validated against a number of tests in which system acceleration time histories were measured. One such example is shown in Fig. 13. The excellent agreement between MIMIC and the experimental

data appears to be fairly typical. One notable exception is for a case involving a 46-ft-diam parachute, which has a porosity that is much larger than the other cases considered. The porosity is, in fact, considerably larger than that recommended by Knacke[40] for good parachute design.

Grid-Based CFD Models

Recently, several researchers have coupled conventional grid-based CFD codes with structural dynamic models of the parachute. While these codes have not been tested extensively and have not been used for routine design work, they nevertheless represent an exciting emergence of a new numerical tool.

In the work of Stein et al.,[44] as well as that of Stein and Benney,[45] the SALE CFD code developed by Amsden et al.[46] was used in conjunction with a simple spring-mass-damper model of the parachute. In the later work[45] an elliptic C-Grid mesh was used to alleviate some of the earlier meshing problems.

Initial computational results of this model compare favorably with experimental data for a half-scale C-9 parachute as evidenced by Fig. 14. Calculated canopy shapes for the time period ($1 < t < 2$) are shown in Fig. 15. The characteristic overinflation is clearly seen. At later times the canopy obtains a more rounded shape with a smaller skirt radius. The authors note that significant enhancements may be required before this coupled code can be used as a routine design tool. For instance, the present code requires one to assume a normal damping coefficient, which has a significant effect on the peak load.

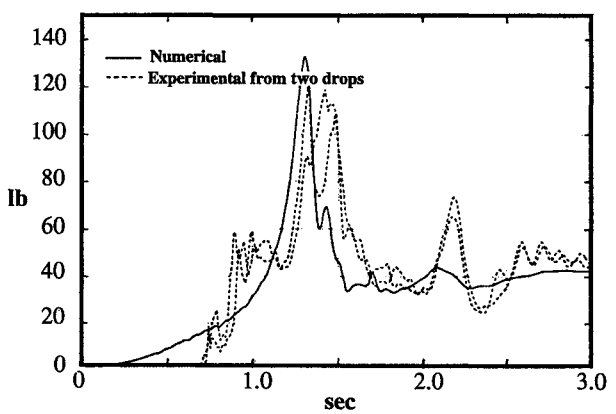

Fig. 14 Experimental and calculated payload force for a half-scale C-9 parachute.[45]

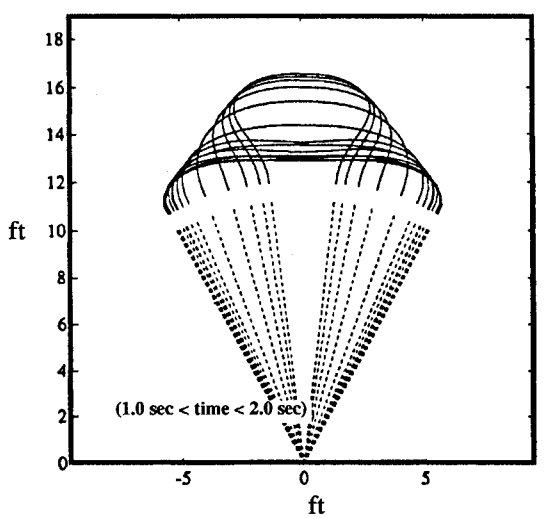

Fig. 15 Calculated canopy shape for a half-scale C-9 parachute.[45]

Haug et al.[47] of Engineering Systems International (ESI) have recently reported on a benchmark simulation of parachute inflation that was achieved by coupling ESI's PAM-FLOW™ and PAM-SOLID™ codes. The flow code is a finite element code developed by Lohner,[48] which uses unstructured Eulerian grids. Near moving boundaries it uses automatic adaptive remeshing based on an arbitrary Lagrange Euler (ALE) formulation.

Geometric shapes of the inflating parachute from this simulation are shown in Fig. 16. Stresses in the fabric were also computed. Comparisons with experimental data were not presented in the indicated reference. Further benchmarking will be required to evaluate the accuracy and computational effort required to provide adequate simulations for design purposes.

An interesting paper by Garrard et al.[49] presents a simulation tool for examining the inflation of a ram air parachute. While we are not dealing explicitly with ram air parachutes in this assessment, it is clear that a code that can model its inflation has important underlying capabilities for simulating the inflation of a ballistic parachute. The flow code is based upon work done by Tezduyar et al.[50]

The inflation process is shown in Fig. 17. During the initial phase of inflation, the parachute is modeled as a rectangular box that expands in both the chordwise and spanwise directions. This box falls under the influence of the suspended payload. The staged opening of the parachute following the initial inflation is modeled by evolving the rectangular box into a curved shape with inflated cells that represents an inflated parafoil. The span of this parafoil increases with time to simulate the sequential opening process. During this stage, the parafoil starts to develop significant lift and begins to glide. The forces and velocities calculated are similar to those measured during flight tests. Simulation was carried out on the Cray T3D massively parallel supercomputer at the University of Minnesota Army High-Performance Computing Research Center.

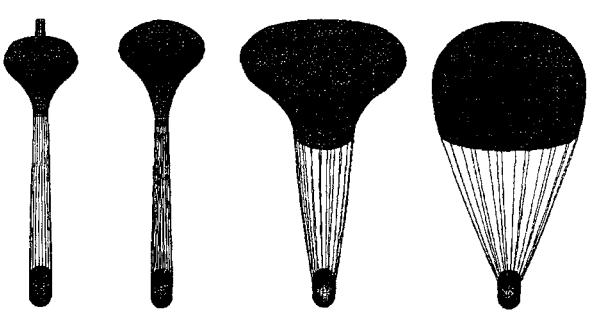

Fig. 16 Parachute deployment benchmark.[47]

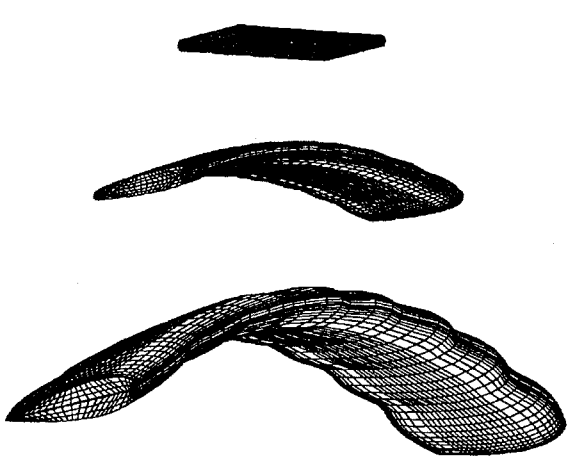

Fig. 17 Ram air parachute inflation simulation.[49]

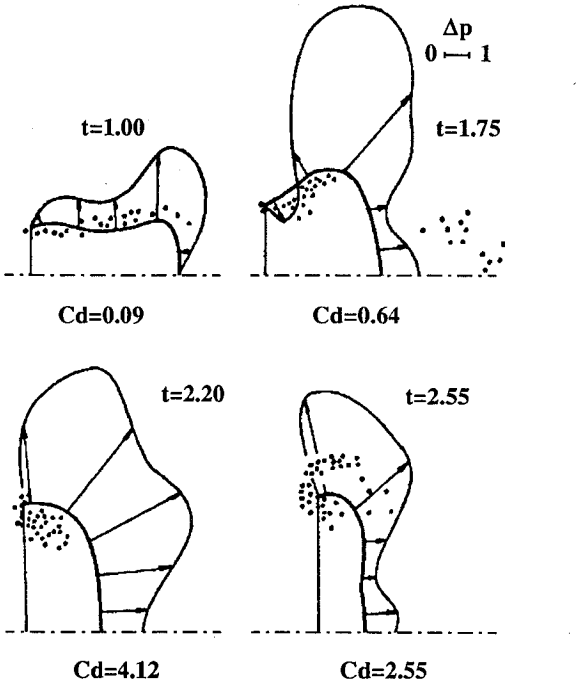

Fig. 18 Parachute inflation using a simple vortex model.[52]

Vortex Models

While vortex models have been applied to a number of bluff bodies, including hemispherical cups, very few attempts have been made to couple them with an inflating parachute structure. McCoy and Werme[51] presented an axisymmetric vortex method in which vortex rings were shed at the canopy skirt. They later extended this work to include the simulation of ringslot and ribbon parachutes in which ring vortices were shed from each ribbon edge. An attempt to couple their model with the dynamics of the canopy was unsuccessful in that the parachute would not open.

Dneprov[52] reports on a very similar vortex model that has been used to successfully model the inflation process. The vortex model used by Dneprov[52] to study the stresses in the fabric of an inflating parachute was originally developed by Belotserkovsky et al.[53] In this simplified model, vortex rings are shed only from the skirt just as in the McCoy and Werme[51] model.

A typical calculation is shown in Fig. 18. The calculation shown in this figure captures the qualitative characteristics of inflation with a peak drag coefficient that is significantly greater than the steady drag coefficient and canopy shapes that appear to be realistic. The drag coefficient reaches a steady value of about 0.8 between a nondimensional time of 7.5–10.0, which is about what one would expect for a solid circular parachute.

Note that secondary separation on the aft side of the canopy is not modeled, since shedding can only take place at the skirt. In some cases this may lead to significant error. It is even possible that the flow will not separate at the skirt, but more nearly at the maximum diameter of the parachute. On the positive side, this simplification reduces the computational time by at least one or two orders of magnitude over models that shed vorticity all along the surface.

Additional Aerodynamic Considerations

Deployment

As mentioned previously, deployment issues are, in most cases, very complicated from an aerodynamic standpoint. Many aerodynamic questions associated with the deployment phase have been solved by using educated guesses along with a test program to arrive at a final design. It would appear, however, that much could be utilized by the parachute community from store separation technology.

Several experimental and numerical techniques have been used to model the separation of stores from aircraft. A 1975 review of store separation is given by Schindel[54] with more recent reviews being given by Dillenius et al.,[55] as well as Wilcox et al.[56] The basic concept behind this technology is to build either a wind-tunnel model, a CFD model, or a vortex panel model of the store and pertinent parts of the aircraft. A number of runs are made with the store at different positions relative to the aircraft. Aerodynamic coefficients of the store are obtained at each position.

There are two or three ways in which the data are obtained and later used in the store separation simulation. In one technique called the grid method, the runs are made with the store at a number of grid points. During the store-separation simulation, interpolated aerodynamic coefficients are available as the store moves through the mesh of grids. Another method is called the captive trajectory method. In this technique, the position to which the store will move during the next time step is calculated based on the aerodynamic coefficients at the present position. The store is then moved to the new position and a new set of aerodynamic coefficients is obtained.

Figure 19 shows an interesting calculation using a panel method for a JP233 dispenser being released from under the wing of a Buccaneer aircraft. This calculation was done after a flight test in which the dispenser impacted the right wingtip and removed the pitot tube.

The use of store separation technology is most beneficial for configurations that have only a few degrees of freedom. A deployment problem that possesses many degrees of freedom, for example, is the line sail problem depicted in Fig. 20. In this problem, the suspension lines have more drag than the pilot parachute because of flow across the lines. The resulting fish hook configuration is detrimental from the standpoint that it may cause unpredictable deployment times, excessive snatch or peak loads, and unreliable inflation of the main parachute. These problems result in loss of system performance at best, and at worst, complete failure of the system.

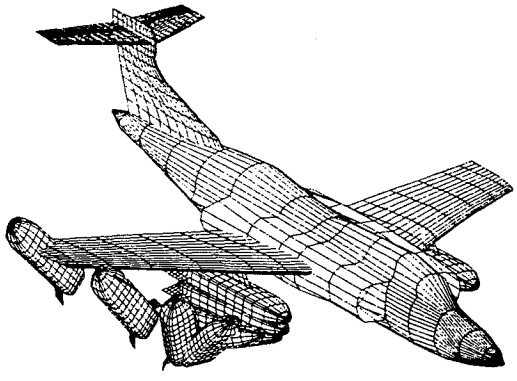

Fig. 19 TSPARV calculation of a JP233 dispenser release from a Buccaneer aircraft.[55]

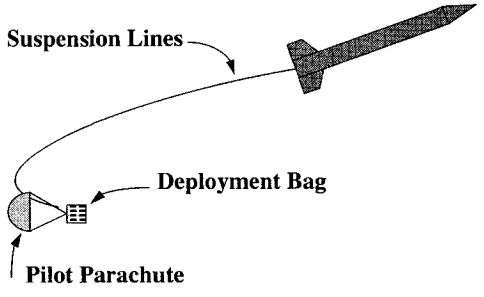

Fig. 20 Line sail.

Moog,[57] Purvis,[58,59] and Sundberg[60] have developed numerical models pertaining to this problem. In each case, the suspension lines and main canopy are modeled as a series of lumped masses connected together by springs. Aerodynamic coefficients are estimated for the suspension line segments. One of the more difficult tasks associated with this model is the simulation of the deployment bag being stripped from the main canopy. According to Maydew and Peterson,[8] the deployment of a particular 46.3-ft main parachute from a four-leaf deployment bag requires 19 different steps.

Terminal Descent

Because of the extensive use of wind tunnels and drop tests for determining terminal descent properties of ballistic parachute systems, a very large body of experimental data exists. Only a few attempts have been made to numerically calculate such flows. The main reason that numerical calculations are not done routinely using grid-based CFD codes is that they tend to be very expensive if the canopy is modeled in any detail. For instance, the 12-gore, 12-ribbon configuration studied by Nelsen[36] required a number of days of Cray CPU time to converge toward a steady solution. For more complex geometries (i.e., more ribbons and gores), finer grids would be required, which would drive the CPU times up even higher. Vortex methods are in a somewhat primitive state of development, but may eventually hold some promise for low Mach number flows since they are gridless and are able to predict the flowfield everywhere based on the vorticity in the wake and in the canopy boundary layers.

We conclude, therefore, that the parachute designer in 1995 must rely primarily on existing test results to characterize the behavior of parachutes in terminal descent. For radically new designs, a wind-tunnel or drop test may be required. A recent review of steady-state aerodynamics is given in Chap. 4 of Maydew's and Peterson's book[8] on parachute design. This chapter provides an excellent review of information that is applicable to terminal descent of a ballistic parachute. We provide the reader with a summary of that material.

Chapter 4 of Maydew's and Peterson's book provides a number of references concerning steady drag measurements made on flat and conical ribbon parachutes. The effects of suspension line length, canopy porosity, number of ribbons, and number of gores on the drag coefficients of these parachutes are presented. Information on the drag coefficients of other configurations such as hemisflo, ringslot, disk-gap-band, guide surface, rotafoil, vortex ring, ballute, and supersonic-X is also referenced. The effect of Mach number on the drag coefficient for a variety of configurations is summarized in Fig. 21.

Maydew and Peterson also reviewed the effects of forebody wakes on drag at subsonic and supersonic speeds, the drag coefficient and comparative static stability of reefed parachutes, and the drag of parachute clusters. They also present a limited amount of experimental pressure distribution data. Finally, they discuss several stability issues including static stability, dynamic stability, and inflation instabilities.

Wake Recontact

Spahr and Wolf[61] discuss the phenomenon of wake recontact using wake momentum considerations. They note that as the parachute system decelerates, the momentum in the wake is in some cases sufficient to cause the parachute to be overtaken by fluid in the wake. This recontact of the wake with the parachute causes a distortion of the canopy shape. Recent work done by Strickland[34] and Higuchi et al.[35] on axisymmetric bluff bodies in decelerating flows shows that vortices shed from the edges of the body move closer to the body during the deceleration phase. These vortices produce a change in the pressure distribution, which is in turn responsible for the distortion of the canopy shape. In severe cases the drag force decreases dramatically, as evidenced by the data shown in Fig. 9 for a disk that is decelerated from some constant velocity to rest.

The most obvious effect of wake recontact is the change in the parachute diameter. Typically, the parachute first overinflates to a diameter that is larger than the steady-state value, then shrinks to a diameter that is less than the final value, and then eventually reaches some steady-state condition. For vertically deployed systems in light winds, the diameter change tends to be symmetric. If the wake recontact occurs on a parachute system, which is in the process of turning over from a horizontal to a vertical flight path, the diameter change is nonsymmetric. In some cases, the canopy may become so distorted that reinflation becomes impossible because of tangling or the flight velocity is too low. Diameter changes can also occur that are unrelated to wake recontact. For instance, for an infinite mass deployment, slight overinflations and underinflations of the canopy may occur shortly after deployment because of the elasticity and mass of the canopy. As mentioned earlier, some parachute systems may puff or breathe during terminal descent producing periodic variations in parachute diameter.

Strickland and Macha[62] conducted a series of tests on a 10-ft-diam ringslot parachute with a geometric porosity of 20% to establish the conditions under which wake recontact occurs. The vertical helicopter drop tests covered a range of mass ratios from 0.5 to 3.0, and a range of Froude numbers from 70 to 400. Data consisted of velocity time histories obtained using a laser tracker, and diameter time histories obtained from photometric data. A collapse parameter R_C based on the ratio of the maximum parachute diameter to the subsequent minimum diameter was correlated with the mass ratio M_R and the Froude number Fr, or equivalently with the initial-to-final velocity ratio V_0/V_t.

The collapse parameter correlation resulting from these tests is shown in Fig. 22. The square, circular, triangular, and diamond symbols correspond to mass ratios of 0.45, 0.95, 1.78, and 3.04, respectively. The collapse parameter $R_{C\infty}$ is from an

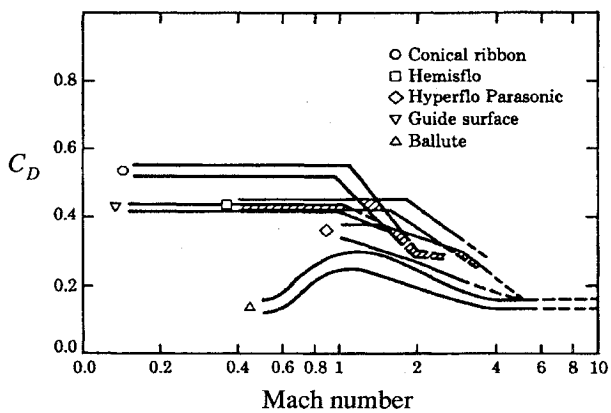

Fig. 21 Drag coefficients vs Mach number.[8]

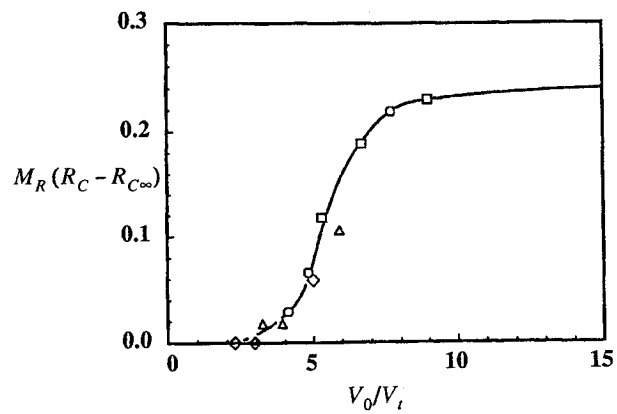

Fig. 22 Collapse parameter correlation.[62]

infinite mass wind-tunnel test and is used to eliminate the effects of diameter change because of elasticity in the system. As can be seen from this figure, significant collapse occurs for velocity ratios in excess of 5.0.

Oler[63] and Yavuz and Oler[64] developed a numerical model for wake recontact based on the solution of an axial momentum equation with a self-similar turbulent wake model. Collapse was based on the occurrence of wake velocities that approached that of the velocity of the parachute. Their results showed that velocity ratios in excess of 4.8–5.7 produced collapse. In their model, the collapse velocity ratio was a weak function of the opening length of the parachute. The longer the opening length, the higher the collapse velocity ratio.

Aircraft Parachute Interaction

Parachute system performance issues such as turnover and wake recontact may be influenced by velocities induced by the wake of the delivering aircraft. The magnitude and direction of these aircraft-induced velocities are dependent on the specific delivering aircraft (as characterized by its size, shape, and weight), the aircraft's speed and flight path (including any maneuvers that it is performing), and the location on the aircraft from which the system is released. In addition, the parachute deployment sequence is of major importance.

The most significant effects will tend to occur after parachute deployment, since induced velocities from the aircraft may become significant when compared to the velocity of the parachute system. For example, any downwash behind an aircraft will tend to cause a parachute system, which is horizontally deployed, to fly at a more positive angle of attack. As the forward speed of the parachute system decreases after deployment, this induced angle of attack will tend to increase. This effect tends to retard the rate at which the parachute system turns over from a horizontal trajectory into a vertical one. On the other hand, a maneuvering aircraft might produce upwash in its wake, which would produce an opposite effect. In this case, the turnover rate would be enhanced. Aircraft-induced velocities may also affect the wake recontact process discussed in the last section. Wake recontact may be either enhanced or diminished, depending upon the aircraft flight path and the parachute deployment sequence.

An approximate method of calculating the wake velocities induced by an aircraft on parachute/payload trajectories was developed by Strickland.[65] In his work, the aircraft wing was represented by a simple lifting line, the strength of which was a function of the specified lift, the wingspan, and the freestream velocity and density. In an extension of that work by Fullerton et al.,[66] the aircraft wing was represented by a number of quadrilateral vortex panels that were used to discretize the aircraft's wing planform. Therefore, the distribution of vorticity is a function of the shape of the wing planform and not just the aircraft wingspan. A schematic of the aircraft and its wake structure is shown in Fig. 23.

The resulting AIVEL-PW code was used to simulate a series of wind-tunnel tests involving a 6% scale model of the B1-B bomber, which were made by Strickland et al.[67] The tests involved measuring wake velocities behind the model for fixed angle-of-attack cases, as well as for cases in which the model executed a pitch-up, pitch-down sequence.

Figure 24 shows contour plots of the vertical component of induced velocity at a crossplane located approximately 0.14 model lengths behind the model from the experimental data and from AIVEL-PW predictions. The model was at a fixed angle of attack of 11 deg for these cases. As the plots show, both the velocity magnitudes and the distribution of the velocity compare well between the data and the predictions, especially near the wingtips. The differences toward the center of the plots may be because of the fact that AIVEL-PW was not able to model effects of the model's fuselage or its engines.

The effects of aircraft downwash on the trajectories of parachute-retarded payloads was investigated by Fullerton et al.,[66]

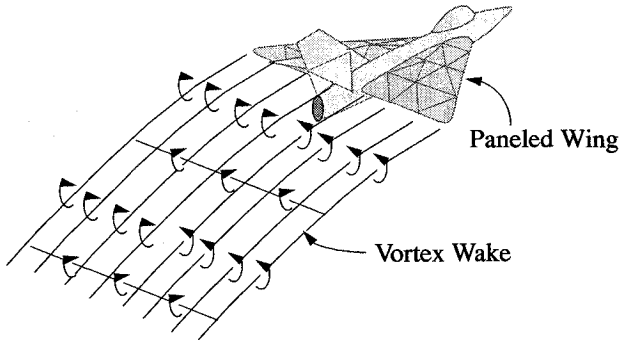

Fig. 23 Aircraft vortex system.[66]

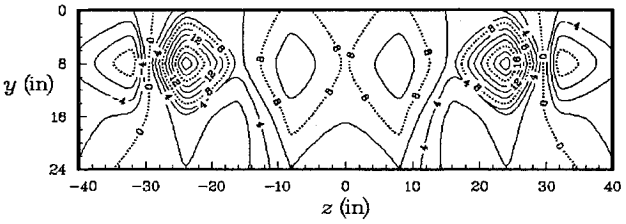

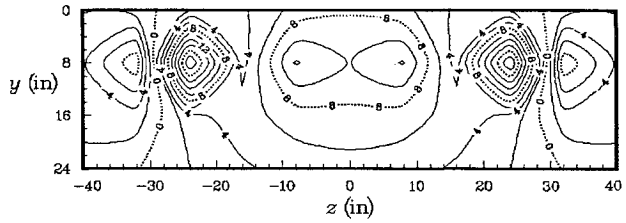

Fig. 24 Vertical velocity contours for B1-B model.[66]

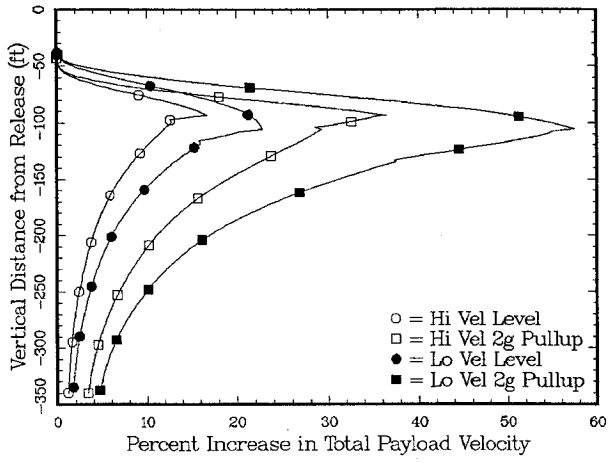

Fig. 25 Increase in total payload with downwash.

using the AIVEL-PW code imbedded in a trajectory code. This investigation was conducted using a two-body trajectory code. The code calculates the trajectory of both the payload and parachute by treating each as a three-degree-of-freedom point mass, with the angular orientation determined by the straight line connecting the two points.

The example calculation shown in Fig. 25 demonstrates the effect on total payload velocity of the aircraft-induced velocities for a 2450-lb payload with a 46.3-ft-diam ribbon parachute being released from a B1-B aircraft. Cases involving two aircraft speeds were considered: 908 and 655 ft/s. The aircraft altitude at release was 340 ft above ground level for all cases. Since the trajectory code does not include deployment of the

parachute, the calculations were started at the time of canopy stretch, approximately 1.0 s after release. At this time the payload is 37 ft below the wing for the higher speed release and 31 ft below the wing for the lower speed release. For all conditions, the payload is 67 ft behind the nose of the aircraft (5 ft behind the leading edge of the paneled wing structure), at the start of trajectory calculations. This initial condition puts the payload far enough below the wing that the downwash velocities on the payload and canopy are already significantly reduced. At each release speed, two aircraft maneuvers are considered: 1) a continuation of straight and level flight, and 2) the initiation of a 2-g pull-up maneuver in the 0.5 s time after canopy stretch (2-g pull up means the lift is three times the aircraft weight).

In determining a minimum release altitude for a given payload, one must consider the impact kinetic energy of the payload. Considering the results of downwash as shown in Fig. 25, it can be seen that impact velocity can be increased with downwash, and significantly so with a maneuver.

A separate example trajectory was calculated for an F-18 aircraft releasing a parachute-retarded 750-lb payload. The release condition was 1070 ft/s and the aircraft continued with straight and level flight. For this example, the calculated effect of the downwash was negligible. The F-18 is a much lighter and smaller aircraft than the B1-B, which therefore, produces much less downwash velocity.

Conclusions

Present State of the Art

At the present time, parachute aerodynamics design is largely an empirical process. On the other hand, numerical-predictive capability associated with parachute aerodynamics is beginning to emerge from the research stage and should begin to have a major impact on the design process within the next decade. A significant trend is the move away from cut-and-try methods or empirically based methods, towards physics-based formulations. We make no attempt in this article to advise the reader as to the availability or user friendliness of various computer codes, as this is changing rapidly and will depend somewhat on the resources available to the individual user.

Recent advances include the following: 1) the ability to make calculations for the fluid flow over complicated parachute canopies, 2) calculations in which the coupling between the fluid flow and the parachute structure have been made, 3) formulation of more sophisticated semiempirical momentum-based inflation models, 4) development of some numerical tools to model the deployment process, and 5) development of preliminary numerical tools to model the interaction between the delivery vehicle and the parachute system.

Future Direction

Because of the possibility of limited test budgets and time constraints associated with the design of parachute systems, the designer of the future needs to have a suite of numerical design tools available to him. These tools must be robust, accurate, and user friendly. To be of maximum value, they must be integrated tools in which the aerodynamic and structural behavior of the parachute system is modeled as well as other aspects of the mission from deployment to impact.

To move the present state of the art forward toward the previously stated set of goals, the following steps should be taken:

1) In the short term, continue to develop user-friendly design tools that rely upon current empirical or semiempirical methods.

2) Continue to develop faster more accurate fluid mechanics solvers.

3) Obtain high-quality laboratory experimental data on unsteady bluff-body or parachute flowfields.

4) Carefully validate and benchmark fluid mechanics solvers against high-quality laboratory data.

5) Develop more sophisticated structural models of parachute canopies that include all pertinent geometry and material properties.

6) Develop robust codes that couple the fluid mechanics and structural behavior of the parachute system.

7) Develop advanced deployment models that include interactions with the delivery vehicle.

8) Develop innovative front-end and back-end software to provide an advanced user-friendly design interface.

Acknowledgment

Work performed by the first author was supported by the U.S. Department of Energy under Contract DE-AC04-94AL85000.

References

[1]Von Eckroth, W., Garrard, W. L., and Miller, N., "Design of a Recovery System for a Reentry Vehicle," AIAA Paper 93-1224, May 1993.

[2]Meiboom, F., "Aerodynamic Characterization and Trajectory Simulations for the Ariane-5-Booster Recovery System," AIAA Paper 93-1214, May 1993.

[3]Behr, V. L., "The Development of a Parachute System for Aerial Delivery from High Speed Cargo Aircraft," AIAA Paper 93-1232, May 1993.

[4]"Performance of and Design Criteria for Deployable Aerodynamic Decelerators," U.S. Air Force ASD-TR-61-579, Dec. 1963.

[5]Ewing, E. G., Bixby, H. W., and Knacke, T. W., "Recovery Systems Design Guide," U.S. Air Force Flight Dynamics Lab.-TR-78-151, Dec. 1978.

[6]Bearman, P. W., "Challenging Problems in Bluff Body Wakes," *IUTAM Symposium of Bluff-Body Wakes, Dynamics and Instabilities*, Springer–Verlag, New York, 1992, pp. 1–10.

[7]Natarajan, R., and Acrivos, A., "The Instability of the Steady Flow Past Spheres and Disks," *Journal of Fluid Mechanics*, Vol. 254, 1993, pp. 323–344.

[8]Maydew, R. C., and Peterson, C. W., *Design and Testing of High-Performance Parachutes*, AGARD-AG-319, Nov. 1991.

[9]Roos, F. W., and Willmarth, W. W., "Some Experimental Results on Sphere and Disk Drag," *AIAA Journal*, Vol. 9, No. 2, 1972, pp. 285–291.

[10]Blevins, R. D., *Applied Fluid Dynamics Handbook*, Reinhold, New York, 1984.

[11]Achenbach, E., "Vortex Shedding from Spheres," *Journal of Fluid Mechanics*, Vol. 62, Pt. 2, 1974, pp. 209–221.

[12]Kim, H. J., and Durbin, P. A., "Observations of the Frequencies in a Sphere Wake and of Drag Increase by Acoustic Excitation," *Physics of Fluids*, Vol. 31, No. 11, 1988, pp. 3260–3265.

[13]Sakamoto, H., and Haniu, H., "A Study on Vortex Shedding from Spheres in a Uniform Flow," *Journal of Fluids Engineering*, Vol. 112, Dec. 1990, pp. 386–392.

[14]Fuchs, H. V., Mercker, E., and Michel, U., "Large-Scale Coherent Structures in the Wake of Axisymmetric Bodies," *Journal of Fluid Mechanics*, Vol. 93, Pt. 1, 1979, pp. 185–207.

[15]Berger, E., Scholtz, D., and Schumm, M., "Coherent Vortex Structures in the Wake of a Sphere and a Circular Disk at Rest and Under Forced Vibrations," *Journal of Fluids and Structures*, Vol. 4, No. 3, 1990, pp. 231–257.

[16]Higuchi, H., "Visual Studies on Wake Behind Solid and Slotted Axisymmetric Bluff Bodies," *Journal of Aircraft*, Vol. 28, No. 7, 1991, pp. 427–430.

[17]Cannon, S. C., "Large-Scale Structures and the Spatial Evolution of Wakes Behind Axisymmetric Bluff Bodies," Ph.D. Dissertation, Univ. of Arizona, Tucson, AZ, 1991.

[18]Roberts, B. W., "Drag and Pressure Distribution on a Family of Porous, Slotted Disks," *Journal of Aircraft*, Vol. 17, No. 6, 1980, pp. 393–401.

[19]Hoerner, S. F., *Fluid-Dynamic Drag*, published by the author, 1965.

[20]Suryanarayana, G. K., Pauer, H., and Meier, G. E. A., "Bluff-Body Drag Reduction by Passive Ventilation," *Experiments in Fluids*, Vol. 16, No. 2, 1993, pp. 73–81.

[21]Bearman, P. W., and Takamoto, M., "Vortex Shedding Behind Rings and Disks," *Fluid Dynamics Research*, Vol. 3, Nos. 1–4, 1988,

pp. 214–218.

[22]Sarpkaya, T., Mostafa, S. M., and Munz, P. D., "Numerical Simulation of Unsteady Flow About Cambered Plates," *Journal of Aircraft*, Vol. 27, No. 1, 1990, pp. 51–59.

[23]Oler, J. W., Lawrence, J. H., and Adamson, T. D., "Unsteady Aerodynamic Loads on Rigid Two-Dimensional Parachutes," Sandia National Labs. Rept. SAND 88-7024, Aug. 1990.

[24]Higuchi, H., "Wake Behind a Circular Disk in Unsteady and Steady Incoming Streams," AIAA Paper 91-0852, April 1991.

[25]Balligand, H., and Higuchi, H., "Experimental Investigation of the Wake Behind a Solid Disk," Sandia National Labs. Rept. SAND 90-7083, Dec. 1993.

[26]Anderson, D. A., Tannehill, J. C., and Pletcher, R. H., *Computational Fluid Mechanics and Heat Transfer*, McGraw–Hill, New York, 1984.

[27]Fletcher, C. A. J., *Computational Techniques for Fluid Dynamics*, Vols. 1 and 2, Springer–Verlag, New York, 1987.

[28]Shyy, W., *Computational Modeling for Fluid Flow and Interfacial Transport*, Elsevier, New York, 1994.

[29]Lewis, R. I., *Vortex Element Methods for Fluid Dynamic Analysis of Engineering Systems*, Cambridge Univ. Press, Cambridge, England, UK, 1991.

[30]Saffman, P. G., *Vortex Dynamics*, Cambridge Univ. Press, Cambridge, England, UK, 1992.

[31]Sarpkaya, T., "Vortex Methods for Flow Simulation," *Advances in Applied Mechanics*, Vol. 31, 1994, pp. 113–247.

[32]Clarke, N. R., and Tutty, O. R., "Construction and Validation of a Discrete Vortex Method for the Two-Dimensional Incompressible Navier-Stokes Equations," *Computers and Fluids Journal*, Vol. 23, No. 6, 1994, pp. 751–783.

[33]Badr, H. M., Coutanceau, M., Dennis, S. C. R., and Menard, C., "Unsteady Flow Past a Rotating Circular Cylinder at Reynolds Numbers 10^3 and 10^4," *Journal of Fluid Mechanics*, Vol. 220, 1990, pp. 459–484.

[34]Strickland, J. H., "Prediction Method for Unsteady Axisymmetric Flow over Parachutes," *Journal of Aircraft*, Vol. 31, No. 3, 1994, pp. 637–643.

[35]Higuchi, H., Balligand, H., and Strickland, J. H., "Numerical and Experimental Investigations of the Unsteady Axisymmetric Flow over a Disk," *Forum on Vortex Methods for Engineering Applications*, Sandia National Labs., Albuquerque, NM, Feb. 1995, pp. 279–297.

[36]Nelsen, J. M., "Computational Fluid Dynamic Studies of a Solid and Ribbon 12-Gore Parachute Canopy in Subsonic and Supersonic Flow," AIAA Paper 95-1558, May 1995.

[37]Sahu, J., Cooper, G., and Benney, R., "3-D Parachute Descent Analysis Using Coupled CFD and Structural Codes," AIAA Paper 95-1580, May 1995.

[38]Rogers, S. E., Kwak, D., and Kiris, C., "Steady and Unsteady Solutions of the Incompressible Navier-Stokes Equations," *AIAA Journal*, Vol. 29, No. 4, 1991, pp. 603–610.

[39]Sundberg, W. D., "New Solution Method for Steady-State Canopy Structural Loads," *Journal of Aircraft*, Vol. 25, No. 11, 1988, pp. 1045–1051.

[40]Knacke, T. W., *Parachute Recovery Systems Design Manual*, Naval Weapons Center NWC TP 6575, Para Publishing, Santa Barbara, CA, March 1991.

[41]Wolf, D. F., "A Simplified Dynamic Model of Parachute Inflation," *Journal of Aircraft*, Vol. 11, No. 1, 1974, pp. 28–33.

[42]McVey, D. F., and Wolf, D. F., "Analysis of Deployment and Inflation of Large Ribbon Parachutes," *Journal of Aircraft*, Vol. 11, No. 2, 1974, pp. 96–103.

[43]Macha, J. M., "A Simple, Approximate Model of Parachute Inflation," AIAA Paper 93-1206, May 1993.

[44]Stein, K. R., Benney, R. J., and Steeves, E. C., "A Computational Model that Couples Aerodynamic and Structural Dynamic Behavior of Parachutes During the Opening Process," U.S. Army Technical Rept. NATICK/TR-93/029, Feb. 1993.

[45]Stein, K. R., and Benney, R. J., "Parachute Inflation: A Problem in Aero-Elasticity," U.S. Army Technical Rept. NATICK/TR-94/015, Feb. 1994.

[46]Amsden, A. A., Ruppel, H. M., and Hirt, C. W., "SALE: A Simplified ALE Computer Program for Fluid Flow at All Speeds," Los Alamos Lab. Rept. LA-8095, June 1980.

[47]Haug, E., Lasry, D., and Kermel, P., "Dynamic Simulation of Industrial Membranes Including Their Interaction with Surrounding Media," Third International Symposium of the SBF 230 Evolution of Natural Structures, Univ. of Stuttgart, Stuttgart, Germany, Oct. 1994.

[48]Lohner, R., "An Adaptive Finite Element Scheme for Transient Problems in Computational Fluid Dynamics," *Computer Methods in Applied Mechanics and Engineering*, Vol. 61, No. 3, 1987, pp. 323–338.

[49]Garrard, W. L., Tezduyar, T. E., Aliabadi, S. K., Kalro, V., Luker, J., and Mittal, S., "Inflation Analysis of Ram Air Inflated Gliding Parachutes," AIAA Paper 95-1565, May 1995.

[50]Tezduyar, T. E., Behr, M., and Liou, J., "A New Strategy for Finite Element Computations Involving Moving Boundaries and Interfaces—The Deforming-Spatial-Domain/Space-Time Procedure: I. The Concept and the Preliminary Tests," *Computer Methods in Applied Mechanics and Engineering*, Vol. 94, No. 3, 1992, pp. 339–351.

[51]McCoy, H. H., and Werme, T. D., "Axisymmetric Vortex Lattice Method Applied to Parachute Shapes," *Proceedings of the AIAA 9th Aerodynamic Decelerator and Balloon Technology Conference*, AIAA, New York, 1986, pp. 140–146 (AIAA Paper 86-2456).

[52]Dneprov, I. V., "Computation of Aero-Elastic Characteristics and Stress-Strained State of Parachutes," *Proceedings of the RAeS/AIAA 12th Aerodynamic Decelerator Systems Technology Conference and Seminar*, AIAA, Washington, DC, 1993, pp. 240–244 (AIAA Paper 93-1237).

[53]Belotserkovsky, S. M., Nisht, M. I., Ponomarev, A. T., and Rysev, O. V., "Computer-Aided Study of Parachutes and Ultra-Light Aircraft," *Izdatel'stvo "Mashinostroenie,"* Translation number: Kirtland-Tr. #21-51, 1987 (in Russian).

[54]Schindel, L. H., "Store Separation," AGARD-AG-202, June 1975.

[55]Dillenius, M. F. E., Perkins, S. C., and Nixon, D., "Pylon Carriage and Separation of Stores," *Tactical Missile Aerodynamics: General Topics*, Vol. 141, Progress in Astronautics and Aeronautics, AIAA, Washington, DC, 1992, pp. 575–666.

[56]Wilcox, F. J., Baysal, O., and Stallings, R. L., "Tangential, Semi-Submerged, and Internal Store Carriage and Separation," *Tactical Missile Aerodynamics: General Topics*, Vol. 141, Progress in Astronautics and Aeronautics, AIAA, Washington, DC, 1992, pp. 667–721.

[57]Moog, R. D., "Aerodynamic Line Bowing During Parachute Deployment," AIAA Paper 75-1381, Nov. 1975.

[58]Purvis, J. W., "Prediction of Parachute Line Sail During Lines-First Deployment," *Journal of Aircraft*, Vol. 20, No. 11, 1983, pp. 940–945.

[59]Purvis, J. W., "Improved Prediction of Parachute Line Sail During Lines-First Deployment," AIAA Paper 84-0786, April 1984.

[60]Sundberg, W. D., "Finite-Element Modeling of Parachute Deployment and Inflation," AIAA Paper 75-1380, Nov. 1975.

[61]Spahr, H. R., and Wolf, D. F., "Theoretical Analysis of Wake-Induced Parachute Collapse," AIAA Paper 81-1922, Oct. 1981.

[62]Strickland, J. H., and Macha, J. M., "Preliminary Characterization of Parachute Wake Recontact," *Journal of Aircraft*, Vol. 27, No. 6, 1990, pp. 501–506.

[63]Oler, J. W., "Prediction of Parachute Collapse Due to Wake Recontact," AIAA Paper 89-0901, April 1989.

[64]Yavuz, T., and Oler, J. W., "Theoretical Modeling of Wake Recontact for a Parachute System," AIAA Paper 93-1219, May 1993.

[65]Strickland, J. H., "An Approximate Method for Calculating Aircraft Downwash on Parachute Trajectories," AIAA Paper 89-0899 April 1989.

[66]Fullerton, T. L., Strickland, J. H., and Sundberg, W. D., "A Vortex Panel Method for Calculating Aircraft Downwash on Parachute Trajectories," AIAA Paper 91-0875, April 1991.

[67]Strickland, J. H., Tadios, E. L., and Powers, D. A., "Wind Tunnel Study of Wake Downwash Behind a 6% Scale Model B1-B Aircraft," Sandia National Labs. Rept. SAND90-0008, May 1990.